GBP2 engages Galectin-9

for immunity against *Toxoplasma gondii*

Elisabeth Kravets[1], Gereon Poschmann[2], Sebastian Hänsch[3], Veronica Raba[1], Stefanie Weidtkamp-Peters[3], Daniel Degrandi[1], Kai Stühler[2,4], Klaus Pfeffer[1*].

[1] Institute of Medical Microbiology and Hospital Hygiene, Heinrich Heine University Düsseldorf, Düsseldorf, Germany

[2] Institute of Molecular Medicine, Proteome Research, Medical Faculty and University Hospital, Heinrich-Heine-University Düsseldorf, Germany

[3] Center of Advanced Imaging, Heinrich Heine University Düsseldorf, Düsseldorf, Germany

[4] Molecular Proteomics Laboratory, Biological and Medical Research Centre (BMFZ), Heinrich-Heine-University Düsseldorf, Düsseldorf, Germany

[*]klaus.pfeffer@uni-duesseldorf.de

Running title: mGBP2 engages Gal9 against *T. gondii*

Corresponding author:

Prof. Dr. Klaus Pfeffer
Institute of Medical Microbiology and Hospital Hygiene
Heinrich Heine University Düsseldorf
Universitätsstr. 1
D-40225 Düsseldorf
Phone: +49 211 81 12459
e-mail: klaus.pfeffer@hhu.de

Abstract

Guanylate binding proteins (GBPs) are large interferon-inducible GTPases, executing essential host defense activities against *Toxoplasma gondii,* an invasive intracellular apicomplexan protozoan parasite of global importance. *T. gondii* establishes a parasitophorous vacuole (PV) which shields the parasite from the host's intracellular defense mechanisms. Murine GBPs (mGBPs) recognize *T. gondii* PVs and assemble into supramolecular mGBP homo- and heterocomplexes that are required for the disruption of the membrane of PVs eventually resulting in the cell-autonomous immune control of vacuole-resident pathogens. We have previously shown that mGBP2 plays an important role in *T. gondii* immune control. Here, to unravel mGBP2 functions, we report Galectin-9 (Gal9) as a critical mGBP2 interaction partner engaged for immunity to *T. gondii*. Interestingly, Gal9 also accumulates and colocalizes with mGBP2 at the *T. gondii* PV. Furthermore, we could prove the requirement of Gal9 for growth control of *T. gondii* by CRISPR/Cas9 mediated gene editing. These discoveries clearly indicate that Gal9 is a crucial factor for the mGBP2 coordinated cell autonomous host defense mechanism against *T. gondii*.

37 **Introduction**

38 After innate immune sensing of pathogens via pattern recognition receptors, production of interferons (IFN) is a key
39 prerequisite for the activation of cell-autonomous immunity, which is essential for the immediate restriction of microbial
40 replication (1, 2). IFN-γ signaling induces the expression of hundreds of interferon-stimulated genes (ISGs) (3-5), which
41 essentially contribute to innate and adaptive immune responses in immune and nonimmune cells (6, 7). Very prominent
42 among IFN-γ ISGs are the members of several families of interferon-inducible GTPases such as the 65- to 73-kDa
43 dynamin-related guanylate-binding proteins (GBPs) (8, 9) and the 45-kDa immunity-related GTPases (IRGs) (10, 11).
44 Human (hGBPs) and murine GBPs (mGBPs) families consist of seven (hGBP1 to hGBP7) and eleven (mGBP1 to
45 mGBP11) members, respectively, which are strongly upregulated in response to IFN-γ (12-14). GBPs characteristically
46 exhibit various cellular functions encompassing antiparasitic, antiviral, and antibacterial activity, as well as inhibitory
47 effects on cell proliferation and tumor suppression (15-26).

48 GBPs display a characteristic multidomain architecture including a large catalytic GTPase (G) domain and a C-terminal,
49 helical domain (8, 27-33). Various mGBPs such as mGBP1, mGBP2, and mGBP7 are especially important effector
50 molecules for the resistance against *Toxoplasma gondii*, an intracellular apicomplexan protozoan parasite of global
51 relevance (16, 25, 34-39). After the active invasion of host cells, *T. gondii* forms a nonfusogenic cytoplasmic
52 membranous structure called the parasitophorous vacuole (PV) in which the parasite efficiently replicates (37, 40, 41).
53 mGBPs are intricately involved in IFN-γ induced growth restriction and killing of the *T. gondii* in murine macrophages,
54 fibroblasts and astrocytes (16, 20, 25, 36, 38, 42). In order to execute their antimicrobial function, mGBPs can
55 specifically associate with pathogen containing compartments of intracellular microbes which encompass pathogen-
56 containing vacuoles (PCVs) as well as viral replication compartments (20, 25, 36, 43-45), resulting in the innate immune
57 detection and cell-autonomous clearing or of PCV-resident pathogens (22, 25, 38, 46). After IFN-γ induction, mGBP2
58 molecules assemble in vesicle like structures (VLS) in the cytoplasm and, after *T. gondii* entry into the host cell, mGBP2
59 attacks the PV membrane (PVM) in orchestrated, supramolecular complexes, ultimately promoting the destruction of
60 PVMs (36, 38). This stage is followed by recruitment of mGBP2 to the plasma membrane of the intracellular parasite,
61 which in turn likely leads to its destruction (38). Multiparameter fluorescence image spectroscopy (MFIS) revealed that

62 mGBP2, on a molecular level, can form homo- or heteromultimers with mGBP1, mGBP3 and, to a lesser extent, with
63 mGBP5 within VLS and at the PVM (38). For PV membrane interactions, isoprenylation / farnesylation and/or
64 hydrophobic moieties in the C-terminus of the GBPs are essential (25, 31, 32, 38, 47). Eventually, especially mGBP2
65 and mGBP7, can be found localized at the parasite cell membrane and inside the targeted parasite (25, 38) probably
66 also interfering with the integrity of *T. gondii* membranes. Importantly, inactivation of mGBP1, mGBP2, or mGBP7 in
67 mice has been shown to result in a vastly impaired resistance to infections with type II *T. gondii* (25, 36).

68 Galectins are a family of lectins characterized by a carbohydrate recognition domain (CRD) with β-galactoside-binding
69 ability (48). Galectins are nucleocytoplasmic proteins, can be exported from cells through a poorly defined
70 unconventional secretion pathway (49) and are able to directly bind to bacteria thereby mediating antibacterial effects
71 and modifying inflammatory signaling events (50). Presently, 15 galectin members have been identified in mammals
72 (51). Immunomodulatory effects of galectins include recruitment of immune cells to the site of infection, promotion of
73 neutrophil function, and stimulation of the bactericidal activity of infected neutrophils and macrophages (48). Previously
74 it has been shown that Gal3 can bind *T. gondii* glycophosphatidylinositols and might be a co-receptor presenting GPIs
75 to TLRs on macrophages (52). Cytoplasmic galectins fulfill functions in several cellular programs including cell growth
76 and apoptosis (53). Through binding to multivalent carbohydrates, galectins can multimerize and thereby cluster these
77 surface glycoconjugates resulting in changes in cell migration, receptor endocytosis and various other cellular events
78 (54, 55). Glycans are largely restricted to the luminal face but absent from the cytosolic face of intracellular vesicles. If
79 vesicular damage occurs, luminal glycans are exposed to the cytosolic milieu, where they can be recognized by
80 galectins (56, 57) . Furthermore, vacuolar instability of bacterial PCVs is recognized by host β-galactoside-binding
81 proteins of the galectin family (50, 58). Intracellular galectins can serve as danger receptors and promote autophagy of
82 the invading pathogen (59).

83 The aim of this study was to explore the molecular interaction(s) that enable mGBP2 to control *T. gondii* replication. By
84 employing immunoprecipitation (IP) followed by mass spectrometry (MS) analysis, we have identified galectin-9 (Gal9)
85 as a novel interaction partner of mGBP2. Furthermore, we demonstrate that the inactivation of Gal9 impairs the cell
86 autonomous IFN-γ induced immune control of *T. gondii* replication.

87

88 **Results**

89 *Identification of Gal9 as mGBP2 interaction partner by IP and MS*

90 Previously, we could show that mGBP2 interacts with itself and other mGBP family members forming homo- and
91 heteromultimers, respectively, in VLS and at the *T. gondii* PVM (38). For a profound understanding of the functions of
92 mGBP2 in *T. gondii* infection, we searched for other interaction partners of mGBP2. To this end, mGBP2$^{-/-}$ murine
93 embryonic fibroblasts (MEFs)(36) expressing HA-tagged mGBP2 were constructed, stimulated with IFN-γ, and either
94 infected with the type II strain *T. gondii* ME49 or left uninfected. An HA-tag specific IP was performed (Fig.S1A) followed
95 by MS based quantitative protein analysis (Fig.1). mGBP2$^{-/-}$ MEFs transduced with an empty expression vector served
96 as negative controls.

97 Statistical analysis revealed that 148 proteins were co-purified with HA-mGBP2 from the uninfected and 294 proteins
98 from the *T. gondii* infected cells. Besides the bait protein mGBP2, further members of the mGBP family were enriched
99 as prey proteins. Among them, a clear co-purification of mGBP1 and mGBP5 which previously were independently
100 identified by MFIS as mGBP2 interacting members, could be observed in uninfected and infected HA-mGBP2
101 expressing MEFs (mGBP1 enrichment factor > 185 in both experimental conditions, mGBP5 enrichment factor 4.8 from
102 uninfected and 15.1 from infected cells) (Fig.1), verifying the reliability of the co-IP and MS analysis.

103 From the list of potential mGBP2 interactors, Gal9 was analyzed further since Gal9 was found significantly enriched in
104 IP samples from type II *T. gondii* ME49 infected cells (Fig.1) and interestingly a role for several other galectin family
105 members had already been proposed in microbial infections (51).

106 To validate and characterize the interactions of Gal9 with mGBP2 in detail, mCherry-fused proteins of Gal9 were co-
107 expressed with full-length mGBP2 or with mGBP2 truncation mutants containing the GTP-binding domain and the
108 middle domain (GM), the middle and the C-terminal effector domain (ME) or the C-terminal effector domain only (E)
109 (31, 36). These cell lines were infected with *T. gondii* followed by co-IP. Using this approach, we could prove the
110 interaction of mGBP2 with Gal9 and could determine a most prominent function of the E-domain of mGBP2 for the
111 interaction with Gal9 (Fig.2 and Fig. S1B).

112

113 *Subcellular localization of Gal9 and recruitment to the T. gondii PV*

114 In a next step, the colocalization of mGBP2 and Gal9 at the PVM of *T. gondii* was determined by confocal (Fig.S2) and
115 Stimulated Emission Depletion (STED) microscopy (Fig.3). Doubly transduced mGBP2$^{-/-}$ MEFs coexpressing GFP-
116 mGBP2 with mCherry-Gal9 were prestimulated with IFN-γ and infected with *T. gondii* ME49 (Fig.3, Fig.S2). GFP-
117 mGBP2 and mCherry-mGBP2 coexpressing MEFs served as a positive control in STED microscopy colocalization
118 experiments (Fig.S3). A distinctive colocalization or close vicinity between mGBP2 and Gal9 could be observed at the
119 PVM already 2 h after infection. Interestingly, mCherry-Gal9 partly colocalized in GFP-mGBP2 containing VLS in
120 uninfected MEFs (Fig.S4). Furthermore, 5-6 h after infection Gal9 and mGBP2 could be found to be located together
121 within the intermembranous space of the PV and eventually within the cytosol of the parasite (Fig.S2). These results
122 indicate that Gal9 is interacting and acting together with mGBP2 and suggest that Gal9 is intricately involved into the
123 cell autonomous immunity mediated by mGBP2.

124

125 *T. gondii replication control by Gal9*

126 Next, the contribution of Gal9 to cell autonomous immunity against *T. gondii* was investigated. For this purpose, the
127 *lgal9* gene was inactivated applying CRISPR/Cas9 gene editing. The inactivation of Gal9 in different clonal NIH 3T3
128 fibroblast cell lines was confirmed by sequencing of the targeted gene loci and, additionally, by Surveyor nuclease
129 assay and WB for Gal9 (Fig.S5). Gal9- deficient fibroblast cell lines were stimulated with IFN-γ and infected with *T.*
130 *gondii* (ME49) and the replication of the parasite was monitored. First, it was determined whether the inactivation of
131 Gal9 leads to increased or decreased infection rates in the targeted cell lines compared to wildtype cells. However, the
132 number of *T. gondii* parasites detected in the gene edited cell lines compared to wildtype fibroblasts did not differ 2 h
133 post infection (Fig.S6). Interestingly, a significant increase in *T. gondii* replication could be observed in fibroblasts
134 harboring an inactivation of Gal9 as determined by qPCR and by quantification of the number of *T. gondii* rosettes and
135 single parasites 24 h after infection (Fig.4, Fig.S7. To assess whether the differences in *T. gondii* control could be
136 attributed to altered cell death, we performed LDH release assays of WT and Gal9 deficient cells including cells

137 reconstituted with the appropriate construct. We could not observe any difference in cell death in Gal9-deficient cells
138 24h after infection (Fig. S8).

139 These results clearly indicate an important role for Gal9 in controlling the intracellular replication of the parasite and
140 suggest that mGBP2 and Gal9 function as supramolecular complexes in the defense against intracellular pathogens.

141

142 **Discussion**

143 mGBP2 provides cell-autonomous immunity to the intracellular PV resident parasite *T. gondii* (31, 36, 38, 44, 60).
144 Although it has been shown that mGBPs translocate to PVs, form supramolecular complexes, attack the membrane of
145 the parasite itself, and, consecutively, restrict replication of the intracellular pathogen, the molecular mechanisms by
146 which mGBPs control the parasite inside the host cell remain largely elusive. Here we identify a novel interaction partner
147 of mGBP2, Gal9, which plays a critical role with respect to the recruitment and in the antiparasitic function of mGBP2
148 in the context of cell-autonomous defense against *T. gondii*.

149 Previously, it was shown that Gal8 colocalizes with mGBP2 positive *Salmonella spp*. in unprimed bone marrow derived
150 macrophages (BMDMs) (61). It was proposed that Gal8 monitors endosomal and lysosomal integrity and detects
151 bacterial invasion of the cytosol by *Listeria* spp. or *Shigella spp.*, serving as a versatile receptor for vesicle-damaging
152 pathogens (61). Interestingly, it was also reported that Gal3, as a member of the Galectin family, and mGBP2 form
153 protein complexes, which associate with vacuoles harboring secretion system-competent *Legionella pneumophila* and
154 *Yersinia pseudotuberculosis* bacteria in response to vacuolar damage (62). In this study we show that, either directly
155 or indirectly, Gal9 interacts and colocalizes with mGBP2 in IFN-γ stimulated MEFs and NIH 3T3 cells in VLS.
156 Considering the methodology used in this study, the possibility exists that Gal9 does not physically interact with mGBP2,
157 but that other proteins/molecules in a complex may be involved in bridging the interaction. However, this would not
158 affect the overall significance of the study. Based on its structural organization, Gal9 belongs to the tandem-repeat type
159 galectins containing two distinct but homologous CRDs (N-CRD and C-CRD) covalently connected by a linker peptide
160 (48, 59). Recruitment of Gal9 to the *T. gondii* PV has not been described previously. Furthermore, Gal9 could not only
161 be found at the PVM but also within the intermembranous space between the PVM and the *T. gondii* plasma membrane
162 as well as in the cytosol of the parasites together with mGBP2 approx. 5-6 h post-infection. This indicates that Gal9 and
163 mGBP2 might recruit to the PVM of *T. gondii* in preformed complexes. Mechanistically, a series of events involving
164 mGBP/IRG mediated PVM indentation, PVM vesiculation/disruption, and parasite plasma membrane stripping, leading
165 ultimately to degradation of the parasite, is proposed by us and others as hallmarks for intracellular *T. gondii* elimination
166 (38, 63, 64). It can be suggested that pore forming or denudating activity of these IFN-γ induced GTPases allows Gal9
167 to transmigrate through the PVM and to recognize β-galactosides on the inner leaflets of the PVM and the parasite,

168 labeling the parasite for further degradation processes. Parasite glycoconjugates play important roles in host cell
169 invasion, and specific interactions between host galectins and parasite glycoconjugates are considered to be critical for
170 pathogen recognition (55). Interestingly, glycosylphosphatidylinositols (GPIs) of *T. gondii* (65) have been shown to be
171 ligands of human Gal3 whereby both glycan and lipid moieties participate in the association of *T. gondii* GPIs with Gal3
172 (52). In this context, Gal3, -8, and -9 bind to host glycans in the luminal side of lysed phagosomes or permeated
173 pathogen vacuoles (66). Intracellular Gal3 was characterized as a sensor of vacuolar rupture that occurs when bacteria
174 such as *Shigella flexneri* or *Salmonella enterica* serovar Typhimurium actively enter the host cell cytosol (58, 67). Gal3,
175 -8 and -9 were also shown to associate with Salmonella-containing vacuoles (SCV) (61, 68, 69). Here we show that
176 Gal9 is required for the control of the parasite *T. gondii*.

177 Functionally, the recruitment of mGBP2 to the PVM was reduced in Gal9- inactivated cells and vice versa; the
178 recruitment of Gal9 to the PVM was reduced in mGBP2 deficient cells. In accordance, significantly fewer Salmonella
179 were targeted by Gal8 in Gbp^{chr3} KO BMDMs than in wild-type BMDMs (70). Also, the delivery of mGBP1 and mGBP2
180 to Legionella-containing vacuoles (LCV) or Yersinia-containing vacuoles is substantially diminished in Gal3- and, to a
181 lesser extent, Gal8-deficient IFN-γ–primed iBMDM (62). In Salmonella-infected cells, SCV rupture and Gal3 recruitment
182 was followed by a rapid and massive recruitment of hGBP1 (67). Interestingly, a specific polybasic protein motif (PBM:
183 KMRRRK) was identified for hGBP1 which is sufficient to drive significant targeting of hGBP1 to *S. flexneri* recognizing
184 exposed glycans from disrupted, bacteria containing, endosomes. Deletion of the PBM-motive leads to substantially
185 reduced colocalization between Gal3-marked vacuoles and hGBP1 (71). mGBP2 lacks such a C-terminal PBM.
186 Nevertheless, the interaction with Gal9 appears to be mostly dependent on the C-terminal domain of mGBP2. Rab GDP
187 dissociation inhibitor α (RabGDIα) acts as a suppressor of the mGBP2-Irga6 axis, hereby the lipid-binding activity of
188 RabGDIα is critical for IFN-γ–induced mGBP2-dependent cell-autonomous immunity against ME49 *T. gondii*. RabGDIα
189 deficiency is accompanied by increased recruitment of mGBP2 and Irga6 to the parasite in MEFs and macrophages
190 and results in enhanced IFN-γ–mediated *T. gondii* clearance *in vitro* and *in vivo* (72). These studies suggest on the
191 one hand GBPs as escorts for distinct anti-pathogenic factors en route to PVs, on the other hand that the recruitment
192 of galectins and GBPs to the PVs might be mutually dependent as part of a coordinated host defense program. This is
193 supported by the significantly increased *T. gondii* proliferation in IFN-γ stimulated Gal9 knock out 3T3 fibroblasts 22h

194 post-infection indicating an important role of Gal9 in cell-autonomous *T. gondii* elimination. In contrast, IFN-γ–primed
195 Gal3$^{-/-}$ BMDMs restricted Yersinia and Legionella bacterial growth, similar to WT BMDMs (62).

196 Thus, it might be speculated that the recognition of the lysed PV by Gal9 initiates the uptake of the parasite into
197 autophagosomes or other degradation pathways as it was described for *Salmonella*, where GBPs promote LC3
198 recruitment via Gal8 (70). Interestingly, *T. gondii* infected Gal3$^{-/-}$ mice develop reduced inflammatory responses in
199 many organs (73) and succumb to an intraperitoneal infection with *T. gondii* associated with a deficient influx of
200 neutrophils and macrophages into the peritoneal cavity (74). The function of Gal9 might be the non-redundant to Gal3
201 and Gal8 in parasitic degradation processes which will be addressed in the future in a Gal9-gene deficient mouse line.

202 The findings of this study indicate that mGBP2 acts as a scaffold organizing the cell autonomous immunity in concert
203 with Gal9 and thus extends the understanding of molecular host responses in the control of intracellular parasites.

204 **Conflict of interest statement**

205 All authors declare that they have no conflicts of interest.

206 **Ethics statement**

207 Not applicable.

208 **Author Contribution statement**

209 EK designed and performed most experiments; GP and KS performed and analyzed the mass spectrometry data; SH
210 and SWP performed STED microscopy and analysis; VR performed LDH-release assays. DD and KP designed and
211 supervised the study. EK, DD and KP wrote the paper. All authors contributed in writing, discussing and editing of the
212 manuscript.

213 **Data availability statement**

214 The mass spectrometry proteomics data have been deposited to the ProteomeXchange Consortium via the PRIDE
215 (107) partner repository with the dataset identifier PXD027029.

216 **Funding statement**

This work was funded by the Deutsche Forschungsgemeinschaft (DFG, German Research Foundation) – Project-ID 233613836 to KP and DD, and Project-ID 267205415 – SFB 1208, Z02 to SWP and SH., and by the Jürgen Manchot Foundation to KP.

Acknowledgements

We thank Julia Mock, Nicole Küpper and Karin Buchholz for excellent technical assistance. We would like to acknowledge the Center for Advanced Imaging (CAi) at Heinrich Heine University for providing access to the Leica TCS SP8 gSTED 3X microscope system (DFG INST 208/665-1 FUGG).

225 1. McNab F, Mayer-Barber K, Sher A, Wack A, O'Garra A. Type I interferons in infectious disease.
226 Nature reviews Immunology. 2015;15(2):87-103.
227 2. Kak G, Raza M, Tiwari BK. Interferon-gamma (IFN-gamma): Exploring its implications in infectious
228 diseases. Biomolecular concepts. 2018;9(1):64-79.
229 3. Boehm U, Klamp T, Groot M, Howard JC. Cellular responses to interferon-gamma. Annual Review
230 of Immunology. 1997;15:749-95.
231 4. Boehm U, Guethlein L, Klamp T, Ozbek K, Schaub A, Futterer A, et al. Two families of GTPases
232 dominate the complex cellular response to IFN-gamma. JImmunol. 1998;161(12):6715-23.
233 5. Martens S, Howard J. The interferon-inducible GTPases. Annual review of cell and developmental
234 biology. 2006;22:559-89.
235 6. Howard JC. Introduction: cell-autonomous immunity. Microbes and infection. 2007;9(14-
236 15):1633-5.
237 7. MacMicking JD. Interferon-inducible effector mechanisms in cell-autonomous immunity. Nature
238 Reviews Immunology. 2012;12(5):367-82.
239 8. Praefcke GJK, Kloep S, Benscheid U, Lilie H, Prakash B, Herrmann C. Identification of residues in
240 the human guanylate-binding protein 1 critical for nucleotide binding and cooperative GTP hydrolysis.
241 Journal of Molecular Biology. 2004;344(1):257-69.
242 9. Praefcke GJK. Regulation of innate immune functions by guanylate-binding proteins. Int J Med
243 Microbiol. 2018;308(1):237-45.
244 10. Zhao YO, Rohde C, Lilue JT, Konen-Waisman S, Khaminets A, Hunn JP, et al. Toxoplasma gondii
245 and the immunity-related GTPase (IRG) resistance system in mice - A Review. Memorias do Instituto
246 Oswaldo Cruz. 2009;104(2):234-40.
247 11. Hunn JP, Feng CG, Sher A, Howard JC. The immunity-related GTPases in mammals: a fast-evolving
248 cell-autonomous resistance system against intracellular pathogens. Mamm Genome. 2011;22(1-2):43-54.
249 12. Cheng YS, Colonno RJ, Yin FH. Interferon induction of fibroblast proteins with guanylate binding
250 activity. JBiolChem. 1983;258(12):7746-50.
251 13. Olszewski MA, Gray J, Vestal DJ. In silico genomic analysis of the human and murine guanylate-
252 binding protein (GBP) gene clusters. Journal of Interferon and Cytokine Research. 2006;26(5):328-52.
253 14. Tripal P, Bauer M, Naschberger E, Mortinger T, Hohenadl C, Cornali E, et al. Unique features of
254 different members of the human guanylate-binding protein family. Journal of Interferon and Cytokine
255 Research. 2007;27(1):44-52.
256 15. Guenzi E, Topolt K, Cornali E, Lubeseder-Martellato C, Jorg A, Matzen K, et al. The helical domain
257 of GBP-1 mediates the inhibition of endothelial cell proliferation by inflammatory cytokines. The EMBO
258 journal. 2001;20(20):5568-77.
259 16. Degrandi D, Konermann C, Beuter-Gunia C, Kresse A, Wurthner J, Kurig S, et al. Extensive
260 characterization of IFN-induced GTPases mGBP1 to mGBP10 involved in host defense. Journal of
261 Immunology. 2007;179(11):7729-40.
262 17. Capaldo CT, Beeman N, Hilgarth RS, Nava P, Louis NA, Naschberger E, et al. IFN-gamma and TNF-
263 alpha-induced GBP-1 inhibits epithelial cell proliferation through suppression of beta-catenin/TCF
264 signaling. Mucosal immunology. 2012;5(6):681-90.
265 18. Kim BH, Shenoy AR, Kumar P, Bradfield CJ, MacMicking JD. IFN-Inducible GTPases in Host Cell
266 Defense. Cell Host & Microbe. 2012;12(4):432-44.
267 19. Nordmann A, Wixler L, Boergeling Y, Wixler V, Ludwig S. A new splice variant of the human
268 guanylate-binding protein 3 mediates anti-influenza activity through inhibition of viral transcription and
269 replication. FASEB journal : official publication of the Federation of American Societies for Experimental
270 Biology. 2012;26(3):1290-300.
271 20. Pilla-Moffett D, Barber MF, Taylor GA, Coers J. Interferon-Inducible GTPases in Host Resistance,
272 Inflammation and Disease. J Mol Biol. 2016;428(17):3495-513.

273 21. Britzen-Laurent N, Herrmann C, Naschberger E, Croner RS, Sturzl M. Pathophysiological role of
274 guanylate-binding proteins in gastrointestinal diseases. World journal of gastroenterology.
275 2016;22(28):6434-43.
276 22. Coers J, Brown HM, Hwang S, Taylor GA. Partners in anti-crime: how interferon-inducible
277 GTPases and autophagy proteins team up in cell-intrinsic host defense. Current opinion in immunology.
278 2018;54:93-101.
279 23. Ghimire D, Rai M, Gaur R. Novel host restriction factors implicated in HIV-1 replication. The
280 Journal of general virology. 2018;99(4):435-46.
281 24. Honkala AT, Tailor D, Malhotra SV. Guanylate-Binding Protein 1: An Emerging Target in
282 Inflammation and Cancer. Front Immunol. 2019;10:3139.
283 25. Steffens N, Beuter-Gunia C, Kravets E, Reich A, Legewie L, Pfeffer K, et al. Essential Role of
284 mGBP7 for Survival of Toxoplasma gondii Infection. mBio. 2020;11(1).
285 26. Yu P, Li Y, Li Y, Miao Z, Peppelenbosch MP, Pan Q. Guanylate-binding protein 2 orchestrates
286 innate immune responses against murine norovirus and is antagonized by the viral protein NS7. J Biol
287 Chem. 2020;295(23):8036-47.
288 27. Praefcke GJK, McMahon HT. The dynamin superfamily: Universal membrane tubulation and
289 fission molecules? Nature Reviews Molecular Cell Biology. 2004;5(2):133-47.
290 28. Prakash B, Praefcke GJ, Renault L, Wittinghofer A, Herrmann C. Structure of human guanylate-
291 binding protein 1 representing a unique class of GTP-binding proteins. Nature. 2000;403(6769):567-71.
292 29. Prakash B, Renault L, Praefcke GJK, Herrmann C, Wittinghofer A. Triphosphate structure of
293 guanylate-binding protein 1 and implications for nucleotide binding and GTPase mechanism. Embo
294 Journal. 2000;19(17):4555-64.
295 30. Ghosh A, Praefcke GJK, Renault L, Wittinghofer A, Herrmann C. How guanylate-binding proteins
296 achieve assembly-stimulated processive cleavage of GTP to GMP. Nature. 2006;440(7080):101-4.
297 31. Kravets E, Degrandi D, Weidtkamp-Peters S, Ries B, Konermann C, Felekyan S, et al. The GTPase
298 Activity of Murine Guanylate-binding Protein 2 (mGBP2) Controls the Intracellular Localization and
299 Recruitment to the Parasitophorous Vacuole of Toxoplasma gondii. Journal of Biological Chemistry.
300 2012;287(33):27452-66.
301 32. Shydlovskyi S, Zienert AY, Ince S, Dovengerds C, Hohendahl A, Dargazanli JM, et al. Nucleotide-
302 dependent farnesyl switch orchestrates polymerization and membrane binding of human guanylate-
303 binding protein 1. Proceedings of the National Academy of Sciences of the United States of America.
304 2017;114(28):E5559-E68.
305 33. Sistemich L, Kutsch M, Hamisch B, Zhang P, Shydlovskyi S, Britzen-Laurent N, et al. The Molecular
306 Mechanism of Polymer Formation of Farnesylated Human Guanylate-binding Protein 1. J Mol Biol.
307 2020;432(7):2164-85.
308 34. Virreira Winter S, Niedelman W, Jensen KD, Rosowski EE, Julien L, Spooner E, et al. Determinants
309 of GBP Recruitment to Toxoplasma gondii Vacuoles and the Parasitic Factors That Control It. Plos One.
310 2011;6(9).
311 35. Yamamoto M, Okuyama M, Ma JS, Kimura T, Kamiyama N, Saiga H, et al. A Cluster of Interferon-
312 gamma-Inducible p65 GTPases Plays a Critical Role in Host Defense against Toxoplasma gondii.
313 Immunity. 2012;37(2):302-13.
314 36. Degrandi D, Kravets E, Konermann C, Beuter-Gunia C, Klumpers V, Lahme S, et al. Murine
315 Guanylate Binding Protein 2 (mGBP2) controls Toxoplasma gondii replication. Proceedings of the
316 National Academy of Sciences of the United States of America. 2013;110(1):294-9.
317 37. Selleck EM, Fentress SJ, Beatty WL, Degrandi D, Pfeffer K, Virgin HW, et al. Guanylate-binding
318 Protein 1 (Gbp1) Contributes to Cell-autonomous Immunity against Toxoplasma gondii. PLoS pathogens.
319 2013;9(4).
320 38. Kravets E, Degrandi D, Ma Q, Peulen TO, Klumpers V, Felekyan S, et al. Guanylate binding
321 proteins directly attack Toxoplasma gondii via supramolecular complexes. Elife. 2016;5.

322 39. Saeij JP, Frickel EM. Exposing Toxoplasma gondii hiding inside the vacuole: a role for GBPs,
323 autophagy and host cell death. Curr Opin Microbiol. 2017;40:72-80.
324 40. Boothroyd JC. Toxoplasma gondii: 25 years and 25 major advances for the field. International
325 journal for parasitology. 2009;39(8):935-46.
326 41. Sibley LD. Invasion and intracellular survival by protozoan parasites. Immunological reviews.
327 2011;240(1):72-91.
328 42. Lubitz FP, Degrandi D, Pfeffer K, Mausberg AK. In Astrocytes the Accumulation of the Immunity-
329 Related GTPases Irga6 and Irgb6 at the Vacuole of Toxoplasma gondii Is Dependent on the Parasite
330 Virulence. Scientific World Journal. 2013.
331 43. Haldar AK, Saka HA, Piro AS, Dunn JD, Henry SC, Taylor GA, et al. IRG and GBP host resistance
332 factors target aberrant, "non-self" vacuoles characterized by the missing of "self" IRGM proteins. PLoS
333 pathogens. 2013;9(6):e1003414.
334 44. Lindenberg V, Molleken K, Kravets E, Stallmann S, Hegemann JH, Degrandi D, et al. Broad
335 recruitment of mGBP family members to Chlamydia trachomatis inclusions. PLoS One.
336 2017;12(9):e0185273.
337 45. Coers J. Self and non-self discrimination of intracellular membranes by the innate immune
338 system. PLoS pathogens. 2013;9(9):e1003538.
339 46. Haldar AK, Foltz C, Finethy R, Piro AS, Feeley EM, Pilla-Moffett DM, et al. Ubiquitin systems mark
340 pathogen-containing vacuoles as targets for host defense by guanylate binding proteins. Proceedings of
341 the National Academy of Sciences of the United States of America. 2015;112(41):E5628-E37.
342 47. Fres JM, Muller S, Praefcke GJK. Purification of the CaaX-modified, dynamin-related large GTPase
343 hGBP1 by coexpression with farnesyltransferase. Journal of Lipid Research. 2010;51(8):2454-9.
344 48. Liu FT, Rabinovich GA. Galectins: regulators of acute and chronic inflammation. Annals of the
345 New York Academy of Sciences. 2010;1183:158-82.
346 49. Haudek KC, Spronk KJ, Voss PG, Patterson RJ, Wang JL, Arnoys EJ. Dynamics of galectin-3 in the
347 nucleus and cytoplasm. Biochim Biophys Acta. 2010;1800(2):181-9.
348 50. Chen HY, Weng IC, Hong MH, Liu FT. Galectins as bacterial sensors in the host innate response.
349 Curr Opin Microbiol. 2014;17:75-81.
350 51. Shi W, Xue C, Su XZ, Lu F. The roles of galectins in parasitic infections. Acta tropica. 2018;177:97-
351 104.
352 52. Debierre-Grockiego F, Niehus S, Coddeville B, Elass E, Poirier F, Weingart R, et al. Binding of
353 Toxoplasma gondii glycosylphosphatidylinositols to galectin-3 is required for their recognition by
354 macrophages. The Journal of biological chemistry. 2010;285(43):32744-50.
355 53. Liu FT, Patterson RJ, Wang JL. Intracellular functions of galectins. Biochim Biophys Acta.
356 2002;1572(2-3):263-73.
357 54. Cerliani JP, Blidner AG, Toscano MA, Croci DO, Rabinovich GA. Translating the 'Sugar Code' into
358 Immune and Vascular Signaling Programs. Trends Biochem Sci. 2017;42(4):255-73.
359 55. Vasta GR. Roles of galectins in infection. Nature reviews Microbiology. 2009;7(6):424-38.
360 56. Coers J. Sweet host revenge: Galectins and GBPs join forces at broken membranes. Cell
361 Microbiol. 2017;19(12).
362 57. Boyle KB, Randow F. The role of 'eat-me' signals and autophagy cargo receptors in innate
363 immunity. Curr Opin Microbiol. 2013;16(3):339-48.
364 58. Paz I, Sachse M, Dupont N, Mounier J, Cederfur C, Enninga J, et al. Galectin-3, a marker for
365 vacuole lysis by invasive pathogens. Cell Microbiol. 2010;12(4):530-44.
366 59. Casals C, Campanero-Rhodes MA, Garcia-Fojeda B, Solis D. The Role of Collectins and Galectins in
367 Lung Innate Immune Defense. Frontiers in immunology. 2018;9:1998.
368 60. Haldar AK, Piro AS, Pilla DM, Yamamoto M, Coers J. The E2-Like Conjugation Enzyme Atg3
369 Promotes Binding of IRG and Gbp Proteins to Chlamydia- and Toxoplasma-Containing Vacuoles and Host
370 Resistance. PloS one. 2014;9(1).

371 61. Thurston TL, Wandel MP, von Muhlinen N, Foeglein A, Randow F. Galectin 8 targets damaged
372 vesicles for autophagy to defend cells against bacterial invasion. Nature. 2012;482(7385):414-8.
373 62. Feeley EM, Pilla-Moffett DM, Zwack EE, Piro AS, Finethy R, Kolb JP, et al. Galectin-3 directs
374 antimicrobial guanylate binding proteins to vacuoles furnished with bacterial secretion systems. Proc
375 Natl Acad Sci U S A. 2017;114(9):E1698-E706.
376 63. Ling YM, Shaw MH, Ayala C, Coppens I, Taylor GA, Ferguson DJ, et al. Vacuolar and plasma
377 membrane stripping and autophagic elimination of Toxoplasma gondii in primed effector macrophages.
378 JExpMed. 2006;203(9):2063-71.
379 64. Martens S, Parvanova I, Zerrahn J, Griffiths G, Schell G, Reichmann G, et al. Disruption of
380 Toxoplasma gondii parasitophorous vacuoles by the mouse p47-resistance GTPases. Plos Pathogens.
381 2005;1(3):187-201.
382 65. Lekutis C, Ferguson DJ, Grigg ME, Camps M, Boothroyd JC. Surface antigens of Toxoplasma
383 gondii: variations on a theme. International journal for parasitology. 2001;31(12):1285-92.
384 66. Mansilla Pareja ME, Bongiovanni A, Lafont F, Colombo MI. Alterations of the Coxiella burnetii
385 Replicative Vacuole Membrane Integrity and Interplay with the Autophagy Pathway. Frontiers in cellular
386 and infection microbiology. 2017;7:112.
387 67. Santos JC, Boucher D, Schneider LK, Demarco B, Dilucca M, Shkarina K, et al. Human GBP1 binds
388 LPS to initiate assembly of a caspase-4 activating platform on cytosolic bacteria. Nat Commun.
389 2020;11(1):3276.
390 68. Pilla DM, Hagar JA, Haldar AK, Mason AK, Degrandi D, Pfeffer K, et al. Guanylate binding proteins
391 promote caspase-11-dependent pyroptosis in response to cytoplasmic LPS. Proceedings of the National
392 Academy of Sciences of the United States of America. 2014;111(16):6046-51.
393 69. Creasey EA, Isberg RR. The protein SdhA maintains the integrity of the Legionella-containing
394 vacuole. Proc Natl Acad Sci U S A. 2012;109(9):3481-6.
395 70. Meunier E, Dick MS, Dreier RF, Schurmann N, Broz DK, Warming S, et al. Caspase-11 activation
396 requires lysis of pathogen-containing vacuoles by IFN-induced GTPases. Nature. 2014;509(7500):366-+.
397 71. Piro AS, Hernandez D, Luoma S, Feeley EM, Finethy R, Yirga A, et al. Detection of Cytosolic
398 Shigella flexneri via a C-Terminal Triple-Arginine Motif of GBP1 Inhibits Actin-Based Motility. mBio.
399 2017;8(6).
400 72. Ohshima J, Lee Y, Sasai M, Saitoh T, Ma JS, Kamiyama N, et al. Role of Mouse and Human
401 Autophagy Proteins in IFN-gamma-Induced Cell-Autonomous Responses against Toxoplasma gondii.
402 Journal of Immunology. 2014;192(7):3328-35.
403 73. Bernardes ES, Silva NM, Ruas LP, Mineo JR, Loyola AM, Hsu DK, et al. Toxoplasma gondii infection
404 reveals a novel regulatory role for galectin-3 in the interface of innate and adaptive immunity. The
405 American journal of pathology. 2006;168(6):1910-20.
406 74. Alves CM, Silva DA, Azzolini AE, Marzocchi-Machado CM, Carvalho JV, Pajuaba AC, et al. Galectin-
407 3 plays a modulatory role in the life span and activation of murine neutrophils during early Toxoplasma
408 gondii infection. Immunobiology. 2010;215(6):475-85.
409 75. Bollineni RC, Koehler CJ, Gislefoss RE, Anonsen JH, Thiede B. Large-scale intact glycopeptide
410 identification by Mascot database search. Sci Rep. 2018;8(1):2117.
411 76. Stratmann B, Engelbrecht B, Espelage BC, Klusmeier N, Tiemann J, Gawlowski T, et al. Glyoxalase
412 1-knockdown in human aortic endothelial cells - effect on the proteome and endothelial function
413 estimates. Sci Rep. 2016;6:37737.
414 77. Grube L, Dellen R, Kruse F, Schwender H, Stuhler K, Poschmann G. Mining the Secretome of
415 C2C12 Muscle Cells: Data Dependent Experimental Approach To Analyze Protein Secretion Using Label-
416 Free Quantification and Peptide Based Analysis. J Proteome Res. 2018;17(2):879-90.
417 78. Perez-Riverol Y, Csordas A, Bai J, Bernal-Llinares M, Hewapathirana S, Kundu DJ, et al. The PRIDE
418 database and related tools and resources in 2019: improving support for quantification data. Nucleic
419 acids research. 2019;47(D1):D442-D50.

420 79. Thevenaz P, Ruttimann UE, Unser M. A pyramid approach to subpixel registration based on
421 intensity. IEEE Trans Image Process. 1998;7(1):27-41.
422 80. Ran FA, Hsu PD, Wright J, Agarwala V, Scott DA, Zhang F. Genome engineering using the CRISPR-
423 Cas9 system. Nature protocols. 2013;8(11):2281-308.

424

425 **Figure legends**

426 **FIGURE 1. Identification of mGBP2 interacting proteins using co-immunoprecipitation in combination with label-**
427 **free quantitative mass spectrometry.** An HA-mGBP2 fusion protein was expressed in mGBP2$^{-/-}$ MEFs. mGBP2$^{-/-}$ MEFs
428 transduced with the empty expression vector were used as controls. MEFs were stimulated with IFN-γ (16h) and left
429 uninfected or were infected with *T. gondii* ME49 for 2h. IPs were performed with an anti-HA antibody from cell lysates.
430 Immunoprecipitated proteins were analyzed by label-free quantitative mass spectrometry. Five to six replicates were
431 analyzed per condition and putative mGBP2 interacting proteins were identified from uninfected and *T. gondii* ME49 infected
432 cells. Mean values of normalized intensities are shown in the bar plots ± standard deviations. In the table, details from the
433 protein identification are shown: the confidence scores from the MASCOT search engine (75, 76), the number of identified
434 unique peptides per protein as well as p-values from Student's t-tests. Furthermore, the enrichment ratios (intensity ratio
435 between mGBP2 expressing cells and vector control) are given (a correction for multiple testing has been performed using
436 the significance analysis of microarray approach, 5% false discovery rate, S_0 0.8, a minimum of 4 valid values per group).

437 **FIGURE 2. Verification of Gal9 as interaction partner of mGBP2 by pulldown analysis.** mGBP2$^{-/-}$ MEFs were
438 reconstituted with GFP-mGBP2 WT or one of the indicated mGBP2 truncation mutants as well as one of the N-terminal
439 mCherry fusion proteins mCherry-mGBP2 or mCherry-Gal9. 10^6 Cells were stimulated with IFN-γ for 16 h and infected
440 with *T. gondii* ME49 for 4h, MOI 50. Cells were lysed and lysate supernatants were incubated o/n with either RFP-Trap®
441 beads (A, B) or with GFP-Trap® beads (C-F) at 4°C. Pull-down (PD) samples and appropriate cell lysate supernatants
442 were subjected to Western Blotting (WB). Blots were stained with α-GFP (A, D, F) or α-mCherry (B, C, E) antibodies.
443 GTP-binding domain (GM), the middle domain and the C-terminal effector domain (ME) or the C-terminal effector
444 domain only (E) (36).

445 **FIGURE 3. Intracellular colocalization of mGBP2 interaction partner Gal9 at the PVM of *T. gondii*.** Recruitment
446 and colocalization of mGBP2 and Gal9 was analyzed after transduction of a GFP-mGBP2 fusion construct in mGBP2^{-}
447 $^{/-}$ MEFs and additional transduction of mCherry-Gal9. MEFs were seeded and incubated on glass slides, stimulated
448 with IFN-γ for 16 h and subsequently infected with *T. gondii* ME49 for 2 h. After fixation, infected cells were treated with
449 an α-RFP V_HH nanobody conjugated to eGFPBoosterAtto647N and with an α-GFP V_HH nanobody conjugated to
450 eGFPBoosterAtto488 for enhancement of the immunofluorescence of mCherry and GFP, respectively. Glass slides
451 were analyzed by STED microscopy. Bars 2 µm. The graphs in the right panel depict a fluorescence intensity analysis
452 of STED images on the far right with the ImageJ software (Fiji) for Atto488 and Atto647 fluorescence signals along the
453 cross sections of PVMs as indicated. The colocalization thresholds were set to 7500-max for the Cherry and 5000-max
454 for GFP in mCherry-Gal9 and GFP-mGBP2 expressing cells.

455 **FIGURE 4. Gal9 is required for the intracellular control of replication of *T. gondii*.** (A) WT and NIH 3T3 cell line
456 clones with verified CRISPR/Cas9 mediated inactivation of Gal9 (see main text and Figs.S5/S6) were stimulated with
457 IFN-γ for 16 h and subsequently infected with *T. gondii* ME49 MOI10 for 24 h. After fixation, *T. gondii* were stained with
458 an α-SAGI antibody and the cell nuclei were labeled with DAPI. Glass slides were analyzed by confocal microscopy.
459 The amounts of rosettes (replicative units) and single parasites inside the PV were determined in WT, Gal9- deficient
460 NIH 3T3 fibroblasts 24 h after infection. In each cell line more than 100 PVs were counted in 3 independent experiments.
461 Mean values ± SD are shown. (B) WT and Gal9 deficient NIH3T3 cells were stimulated with IFN-γ for 16 h and
462 subsequently infected with *T. gondii* ME49 MOI10 for 24 and 48h. Genomic DNA from these samples was extracted
463 and a *T. gondii* specific qPCR was performed. Parasite equivalents per 500 ng DNA are depicted for at least 10
464 individual samples from three independent experiments. Statistical analysis was performed using the Student's t-test.
465 ***: $p <= 0.001$; **: $p <= 0.01$; *: $p <= 0.05$.

466 **FIGURE S1. Identification and validation of mGBP2 interaction partners.** (A) mGBP2$^{-/-}$ MEFs were reconstituted
467 with HA-mGBP2 or a control vector and stimulated with IFN-γ for 16 h. $1x10^6$ cells were infected for 2 h with *T. gondii*
468 ME49 (MOI 50) or left uninfected. Subsequently, cells were lysed and lysate supernatants were incubated o/n with α-
469 HA antibody coupled agarose beads at 4°C for IP. One part of IP samples was separated via 10% SDS-PAGE and

470 labelled using silver staining. Another part of the IP samples was subjected to Western Botting and immune staining
471 with an α-mGBP2 antiserum or an α-HA antibody. A third part of these IP samples was transferred to the MS analysis
472 (see main text).

473 (B) mGBP2$^{-/-}$ MEFs were reconstituted with GFP-mGBP2 WT as well as one of the N-terminal mCherry fusion proteins
474 mCherry-mGBP2, or mCherry-Gal9. mCherry-Control 1, mCherry Control 2, and mCherry-Control 3 are interacting
475 proteins that will be published elsewhere and do not relate to this study. Cells were stimulated with IFN-γ for 16 h and
476 infected with of *T. gondii* ME49 for 4h. Cells were lysed, and lysate supernatants were incubated o/n with GFP-Trap®
477 beads at 4°C. Pulldown samples and appropriate cell lysate supernatants were subjected to Western Blotting. Blots
478 were stained with α-GFP or α-mCherry antibodies.

479 **FIGURE S2. Localization of Gal9 and mGBP2 at *T. gondii*.** Recruitment and colocalization of mGBP2 was analyzed
480 in GFP-mGBP2 expressing mGBP2$^{-/-}$ MEFs with additional transduction of either mCherry-Gal9. MEFs were stimulated
481 with IFN-γ for 16 h and subsequently infected with *T. gondii* ME49 for 5 h. After fixation, *T. gondii* were stained with an
482 α-SAG1 antibody and the cell nuclei were labeled with DAPI. Glass slides were analyzed by confocal microscopy. Bars
483 2 µm.

484 **FIGURE S3. Colocalization of mCherry-mGBP2 and GFP-mGBP2 at the PV membrane of *T. gondii*.** Recruitment
485 and colocalization of mGBP2 was analyzed in GFP-mGBP2 expressing mGBP2$^{-/-}$ MEFs with additional transduction of
486 mCherry-mGBP2 as control. MEFs were stimulated with IFN-γ for 16 h and subsequently infected with *T. gondii* ME49
487 for 2 h. After fixation, *T. gondii* were stained with an α-SAG1 antibody. Infected cells were treated with anti-RFP V_HH
488 nanobody conjugated to eGFPBoosterAtto647N and with anti-GFP V_HH nanobody conjugated to eGFPBoosterAtto488
489 for enhancement of immunofluorescence of mCherry and GFP respectively. Glass slides were analyzed by STED
490 microscopy. Bars 2 µm. The graphs depict a colocalization analysis of STED images with the ImageJ software (Fiji) for
491 GFP and mCherry fluorescence. The colocalization thresholds were set to 13000-max for the Cherry and 2000-max
492 for GFP in mCherry-mGBP2 and GFP-mGBP2 expressing cells.

493 **FIGURE S4. Intracellular colocalization of mGBP2 with the interaction partners Gal9**. Colocalization of GFP-
494 mGBP2 with mCherry-Gal9 was analyzed in mGBP2$^{-/-}$ MEFs reconstituted with the indicated fusion proteins. Cells were

495 stimulated with IFN-γ for 16 h. After fixation, cell nuclei were labeled with DAPI. Glass slides were analyzed by confocal
496 microscopy. Bars 5 µm. The right column depicts the results for a colocalization analysis using the Image Visualization
497 and Analysis Software (Imaris) for GFP and mCherry fluorescence.

498 **FIGURE S5. CRISPR/Cas9 gene editing of Gal9 and verification of Gal9 inactivation.** (A) CRISPR/Cas9 and
499 sgRNA specific for Gal9 were expressed in NIH 3T3 fibroblasts. Clones were picked and DNA from WT and three
500 CRIPR/Cas9 Gal9 targeted cell clones of NIH 3T3 fibroblasts was isolated, PCR amplified (923 bp). PCR products were
501 cloned into the pCR2.1 TA-cloning vector. The Gal9 mutations were verified by Sanger sequencing. Indels, AA
502 sequence and premature stop codons (*) are indicated. (B) For independent mutation analysis, the Surveyor® Mutation
503 Detection Kit for Standard Gel Electrophoresis was employed. Here, a mismatch-specific DNA endonuclease to scan
504 mutations and polymorphisms in heteroduplex DNA is used. PCR amplicons from Gal9 mutant NIH 3T3 clones (test)
505 and WT (reference) DNA were hybridized and the mixtures of hetero- and homo-duplexes were submitted to Surveyor
506 Nuclease digestion. The reference DNA alone, treated similarly, served as a negative control. DNA fragments were
507 analyzed by agarose gel electrophoresis. The formation of new cleavage products, due to the presence of one or more
508 mismatches, is indicated by the presence of additional bands. The relative size of these cleavage products indicates
509 the location of the mismatch or mismatches. (C) Lysate supernatants of NIH 3T3 cells from different CRISPR/Cas9
510 Gal9 sgRNA targeted clones and from WT cells were analyzed by WB. Cells were stimulated with IFN-γ for 16 h. Blots
511 were stained with α-Gal9 antibodies.

512 **FIGURE S6. Inactivation of Gal9 does not influence infection rates of *T. gondii*.** The infection rates of *T. gondii*
513 ME49 were analyzed in WT and independent NIH 3T3 cell line clones with verified Gal9 inactivation. Cells were
514 stimulated with IFN-γ for 16 h and subsequently infected with *T. gondii* ME49. After fixation, *T. gondii* were stained with
515 the α-SAGI antibody and the cell nuclei were labeled with DAPI. Glass slides were analyzed by confocal microscopy.
516 Bars, 5 µm. The amounts of parasites per cell were quantified 2 h after infection.

517 **FIGURE S7. Gal9 is required for the intracellular control of replication of *T. gondii*.** WT and independent NIH 3T3
518 cell line clones with verified CRISPR/Cas9 mediated inactivation of Gal9 (see main text and Figs.S5) were stimulated
519 with IFN-γ for 16 h and subsequently infected with *T. gondii* ME49 for 24 h. After fixation, *T. gondii* were stained with

520 an α-SAGI antibody and the cell nuclei were labeled with DAPI. Glass slides were analyzed by confocal microscopy.
521 Bars, 5 µm.

522 **FIGURE S8. Cell death of Gal9 deficient cells in *T. gondii* infection.** WT and independent NIH 3T3 cell line clones
523 with verified CRISPR/Cas9 mediated inactivation of Gal9 (see main text and Figs.S5) and NIH 3T3 cell line clones with
524 verified CRISPR/Cas9 mediated inactivation of Gal9 reconstituted with mCherry-Gal9 were stimulated with IFN-γ for 16
525 h and subsequently infected with *T. gondii* ME49 for 24 h. Subsequently, an LDH release assay was performed. Positive
526 controls were obtained by treating the cells with 1mM Staurosporine for 24h. Shown are three independent experiments,
527 which were respectively performed in technical triplicates to minimize pipetting errors. Plotted are means +/- SD.
528 Statistical analysis was performed using one-way ANOVA followed by Dunnett's multiple comparison test.; *: $p <= 0.05$.
529 Only statistically significant comparisons were labelled.

530

531 **Experimental Procedures**

532 *Expression Constructs.*

533 The WT ORF of mGBP2 (NCBI accession numbers: mGBP-2, NM_010260.1) was cloned either into the pWPXL
534 plasmid (Trono lab) as N-terminal GFP-fusion constructs or into the pWPI Plasmid (Trono lab) in frame with a N-terminal
535 HA-tag. For the cloning of mCherry constructs (36), the pWPXL plasmid was modified by exchanging of the gene for
536 GFP by the gene for mCherry (38). mRNA was isolated from freshly prepared WT MEFs prestimulated with IFN-γ and
537 infected with *T. gondii*. The ORFs of Galectin 9 (NM_010708.2) was amplified by PCR and then cloned into the modified
538 pWPXL plasmid as N-terminal mCherry-fusion constructs (38). The lentiviral envelope vector pLP/VSVG (Invitrogen)
539 and the packaging vector psPAX2 (Trono lab) were used for the lentiviral genetic transfer.

540 *Cell culture and transduction.*

541 NIH 3T3 fibroblasts (Public Health England; AccNo 93061524) and MEFs were cultured in Dulbecco's modified Eagle's
542 medium (DMEM, Invitrogen/Gibco) supplemented with 10% (v/v) heat-inactivated low endotoxin fetal bovine serum
543 (FBS, Cambrex), 100 U/ml penicillin, 100 µg/ml streptomycin, 2 mM L-glutamine (Biochrom) and 0.05 mM β-
544 mercaptoethanol (Invitrogen/Gibco). Human foreskin fibroblasts (HS27, ATCC CRL-1634) were hold in culture in
545 Iscove's Modified Dulbecco's Medium (IMDM, Invitrogen/Gibco) with the same supplementations. 293FT cells (Gibco,
546 ThermoFisher; R700-07) were cultivated in DMEM supplemented with 10% FBS, 100 U/ml penicillin, and 100 µg/ml
547 streptomycin. All recombinant lentiviruses were produced by transient transfection of 293FT cells according to
548 jetPRIME® transfection protocol (Polyplus, New York City) (38). NIH 3T3 cells and MEFs were seeded in 24 well plates
549 (Corning Incorporated, Germany) and transduced with 600 µl of lentivirus with 25 µg Polybrene
550 (Merck Millipore, Germany). After 5 h of incubation medium was changed. The transduction efficacy was analyzed by
551 flowcytometry. Subsequently, only GFP or double GFP and mCherry positive cells were sorted and cultivated.

552 *In Vitro Passage of Toxoplasma gondii.*

553 Tachyzoites from *T. gondii* strain ME49 (ATCC 50611) were maintained by serial passage in confluent monolayers of
554 HS27 cells. After infection of fibroblasts, parasites were harvested and passaged as described previously (16).

555 *Infection of murine MEFs with T. gondii.*

556 Cells were stimulated with 200 U/mL IFN-γ (R&D Systems, Minneapolis, MN) 16 h before infection. For
557 immunofluorescence, NIH 3T3 fibroblasts and MEFs were cultured in 24-well plates (Falcon, BD
558 Biosciences, Germany) on cover slips (ø 13 mm, VWR International, Germany) and inoculated with freshly harvested
559 *T. gondii* at a parasites/cell ratio of 10:1. To remove extracellular parasites, cells were washed with PBS.

560 *Pull-Down and co-immunoprecipitation analysis of mGBP2*

561 For co-immunoprecipitation experiments, mGBP2$^{-/-}$ MEFs reconstituted with HA-mGBP2 were used. mGBP2$^{-/-}$ MEFs
562 transduced with the empty pWPI vector were used as control cells. 10^6 Cells were then stimulated with IFN-γ for 16 h,
563 infected with the *T. gondii* strain ME49 (MOI50) for 2 h or left uninfected, subsequently lysed and lysate supernatants
564 were incubated o/n with monoclonal mouse anti-HA- antibody coupled to agarose beads (clone HA-7, Sigma-Aldich,
565 USA) at 4°C. IP probes were subjected to silver staining and to Western Blotting. Blots were stained with the mGBP2-
566 specific antiserum (Eurogentec), mouse α-GFP (clones 7.1 and 13.1, Roche, Switzerland) and rabbit αHA (polyclonal,
567 Sigma-Aldrich, USA) antibodies. For pull-down experiments, lysate supernatants of mGBP2$^{-/-}$ MEFs reconstituted either
568 with WT GFP-mGBP2 or GFP-fused truncated mutants mutants or just transduced with a GFP expressing vector, as
569 an appropriate control and coexpressing mCherry fused with Gal9 or just the mCherry protein, were incubated o/n with
570 RFP-Trap® or GFP-Trap® beads (ChromoTek GmbH, Germany) at 4°C. IP probes were subjected to Western Blotting.
571 Blots were stained with the mouse α-GFP or α-mCherry (Clontech, EU) antibodies.

572 *MS Analysis of interaction partners of mGBP2*

573 A label-free mass spectrometry, based quantification approaches enabled by a highly reproducible and stable LC-
574 MS/MS system was chosen for a quantitative analysis of the mGBP2 interactome. Six individual replicates of co-
575 immunoprecipitation samples per group (HA-mGFP2, control-vector, HA-mGFP2 + ME49 and control-vector + ME49)
576 were prepared from transfected IFNγ stimulated mGBP2$^{-/-}$ MEFs (see above). Samples were prepared for mass
577 spectrometric analysis essentially as described elsewhere (77). Briefly, proteins were stacked into an acrylamide gel
578 (about 4 mm running distance), subjected to silver staining, de-stained, reduced and alkylated and digested with trypsin.
579 Resulting peptides were extracted from the gel and approximately 500 ng peptides prepared in 0.1% trifluoroacetic acid
580 for liquid chromatography and mass spectrometric analysis.

581 First, peptide samples were separated on an UltiMate 3000 RSLCnano chromatography system (Thermo Fisher
582 Scientific). Peptides were initially trapped on a 2 cm long trap column (Acclaim PepMap100, 3 µm C18 particle size,
583 100 Å pore size, 75 µm inner diameter, Thermo Fisher Scientific) for 10 min at a flow rate of 6 µl/min with 0.1 % (v/v)
584 TFA as mobile phase. Subsequently, they were separated on a 25 cm long analytical column (Acclaim PepMapRSLC,
585 2 µm C18 particle size, 100 Å pore size, 75 µm inner diameter, Thermo Fisher Scientific) at 60°C using a 2 h gradient
586 from 4 to 40% solvent B (solvent A: 0.1% (v/v) formic acid in water, solvent B: 0.1% (v/v) formic acid, 84% (v/v)
587 acetonitrile in water) at a flow rate of 300 nl / min.

588 Separated Peptides were injected with distal coated SilicaTip emitters (New Objective, Woburn, MA, USA) into an
589 Orbitrap Elite mass spectrometer via a nanosource electrospray interface. The mass spectrometer was operated in
590 positive, data dependent mode with a spray voltage of 1.4 kV and capillary temperature of 275°C. First, a full scan from
591 m/z 350 to 1700 was recorded with a resolution of 60000 (at 400 m/z) in the obitrap analyser with a target for automatic
592 gain control set to 1000000 and a maximal ion time of 200 ms. Then, up to 20 two- and threefold charged precursor
593 ions with a minimal signal of 500 were isolated (isolation width 2) in the linar ion trap part of the instrument. Here, ions
594 were collected for a maximum of 50 ms with an automatic gain control set to 30000, fragmented by collision induced
595 dissociation with a normalized collision energy of 35 and analysed at a resolution of 5,400 (at 400 m/z). Already
596 fragmented precursors were excluded from fragmentation for the next 45 seconds.

597 Quantitative analysis of MS1 based precursor ions was carried out with Progenesis QI for proteomics (version 2.0,
598 Nonlinear Dynamics, Newcastle upon Tyne, UK). The software first detects and aligns precursor ion signals (features)
599 then associates information from MS2 based precursor identification and finally computes protein intensities on basis
600 of associated features. Automatic processing was used without manual alignment adjustment. Here, one run of the
601 control-vector + ME49 could not automatically aligned and was not further considered in the analysis. Searches were
602 triggered by Proteome Discoverer (version 1.4.1.14, Thermo Scientific) and the percolator node was used for
603 identification validation at 1% false discovery rate. Spectra were searched with the Mascot search engine (version
604 MASCOT 2.4.1, Matrix Science, London, UK) considering cysteine carbamidomethylation as fixed and protein N-
605 terminal acetylation and methionine oxidation as variable modification as well as tryptic cleavage specificity with a
606 maximum of two missed cleavage sites. Mass precision was set to 10 ppm for precursor and 0.4 Da for fragment

607 spectra. Database searches were carried out using the mus musculus (UP000000589) and toxoplasma gondii
608 (UP000002226) reference proteome data sets downloaded on 18th January 2018 from UniProtKB including 52548
609 respectively 8404 entries. Only "high confident" peptide spectrum matches were used for further processing and peptide
610 spectrum matches associated with proteins identified with at least two unique peptides. As we noticed a bias towards
611 higher protein intensities in the mGBP2 overexpressing cells (arising from mGBP2 and associated proteins), no global
612 normalization was performed but a normalization of protein intensities based on the sum of the Ig heavy chain proteins
613 P18525, P18524. Calculated protein intensities were further processed within the Perseus (version 1.6.2.2, MPI for
614 Biochemistry, Planegg, Germany) software environment. Here, Student's t-tests were calculated on log2 transformed
615 normalized intensities using the significance analysis of microarrays method for cutoff determination (S_0 set to 0.8, 5%
616 false discovery rate, a minimum of 4 valid values per group). The mass spectrometry proteomics data have been
617 deposited to the ProteomeXchange Consortium via the PRIDE(78) partner repository with the dataset identifier
618 PXD027029.

619 *Immunofluorescence analysis.*

620 Cells were fixed in 4% paraformaldehyde (PFA, Sigma-Aldrich, Germany) permeabilized with 0.02% saponin
621 (Calbiochem-Merck) and blocked in 0.002% saponin with 2% goat serum (DaKoCytomation, Denmark). The outer
622 membrane of T. gondii was visualized by anti-SAG1 (Abcam, UK) at a concentration of 1/700. As secondary reagents,
623 1/200 concentrated Alexa Fluor™ 633-conjugated goat anti-mouse IgG (H+L) (Invitrogen, ThermoFisher Scientific,
624 USA) and Cy3-conjugated goat anti-mouse IgG plus IgM (Jackson ImmunoResearch Laboratories, UK) were used.
625 Nuclei were counterstained with 1/2500 4',6-diamidino-2-phenylindole (DAPI, Invitrogen, ThermoFisher Scientific,
626 USA). The cover slips were fixed in fluorescence mounting medium (Fluoromount-G, Southern Biotechnology
627 Associates, Birmingham, AL). Fluorescence was visualized using a LSM780 confocal microscope (Zeiss, Germany).
628 Image analysis and processing was performed with the ZEN (Zeiss, Switzerland) software.

629 *Gated Stimulated Emission Depletion measurement*

630 Gated Stimulated Emission Depletion (STED) measurements were performed using a TCS SP8 STED 3X (Leica,
631 Wetzlar, Germany) equipped with an HC PL APO CS2 93x glycerol objective (Leica, Wetzlar, Germany, NA 1.3) at a

632 scan speed of 1400 Hz. For the acquisition of the gated STED signal of the eGFPBoosterAtto488, 488 nm was used
633 as the excitation laser line, 592 nm as the corresponding depletion laser line and the hybrid detector range was set
634 from 498 nm to 580 nm with a 1 ns to 6 ns time gating. For the acquisition of the gated STED signal of the
635 mRFPBoosterAtto647N, 633 nm was used as the excitation laser line, 755 nm as the corresponding pulsed depletion
636 laser line and the hybrid detector range was set from 640 nm to 750 nm with a 0.8 ns to 6 ns time gating. Detection of
637 the different signals was carried out in a frame sequential measurement setup. Deconvolved data of gated STED
638 measurements were calculated using Huygens software (Huygens professional, Scientific Volume Imaging,
639 Netherlands) with reduced signal to noise factor of 5 for eGFPBoosterAtto488 and 6 for mRFPBoosterAtto647N and a
640 reduced iteration setting of 20 for both channels. Resulting deconvolved images were visually compared to the raw data
641 to ensure the quality of the calculation. To correct for channel shift, a reference double staining of nuclear pores was
642 acquired with similar settings and utilized as a reference for channel shift correction by the Fiji-plugin "multistackreg"
643 (79).

644 *CRISPR/Cas9 knock out strategy.*

645 The Galectin 9 gene (lectin, galactose binding, soluble 9, *lgals9*) was disrupted by applying the CRISPR/Cas9
646 technology in NIH 3T3 fibroblasts (80). The knock out was performed by transfection of the pSpCas9(BB)-2A-GFP
647 (PX458) plasmid (Addgene, USA), expressing a sgRNA (Gal9: for CAC CGC GGG TTA ATG TAT GGA GAC T, rev
648 AAA CAG TCT CCA TAC ATT AAC CCG C) corresponding to the sequence contained in the first exon of the*lgals9*
649 gene. The sgRNA encoding plasmids were transfected into NIH 3T3 fibroblasts according to jetPRIME^{R} transfection
650 protocol (Polyplus, New York City). The transfection efficacy was analyzed by flow cytometry. Subsequently, GFP
651 positive cells were sorted and single cell colonies were cultivated. Mutated clones of the *lgals9* gene were identified by
652 Surveyor® Mutation Detection (Integrated DNA Technologies, Inc., USA) (for AAC TAG ATT GGG CCT GCC TC, rev
653 AGA GAT CCC CCT GAC TCT GT, expected fragments, expected PCR fragment: 923 bp, expected digested
654 fragments: 747, 176 bp). The knockout of *lgals9*was confirmed by PCR amplification, subcloning and sequencing of the
655 corresponding gene stretches from different single cell colonies. Additionally, WB analysis was performed with a
656 polyclonal rabbit anti-mouse antibody against Gal9 (ARP54821_P050, Aviva Systems Biology).

657 *LDH release assay.*

658 Cell death was quantified by measuring LDH release, using the Invitrogen™ CyQUANT™ LDH Cytotoxicity Assay. For
659 this $3x10^4$ cells of the indicated cell lines were stimulated with 100U/ml IFNγ for 16h. Then cells were infected with *T.*
660 *gondii* ME40 with an MOI of 6.6 for 24h. As positive control, cells were treated with staurosporin for 24h as indicated.
661 % of LDH release was calculated as follows: ((experimental LDH activity- spontaneous LDH activity) x 100) / (maximum
662 LDH activity – spontaneous LDH activity). Each experiment was performed with three technical replicates.

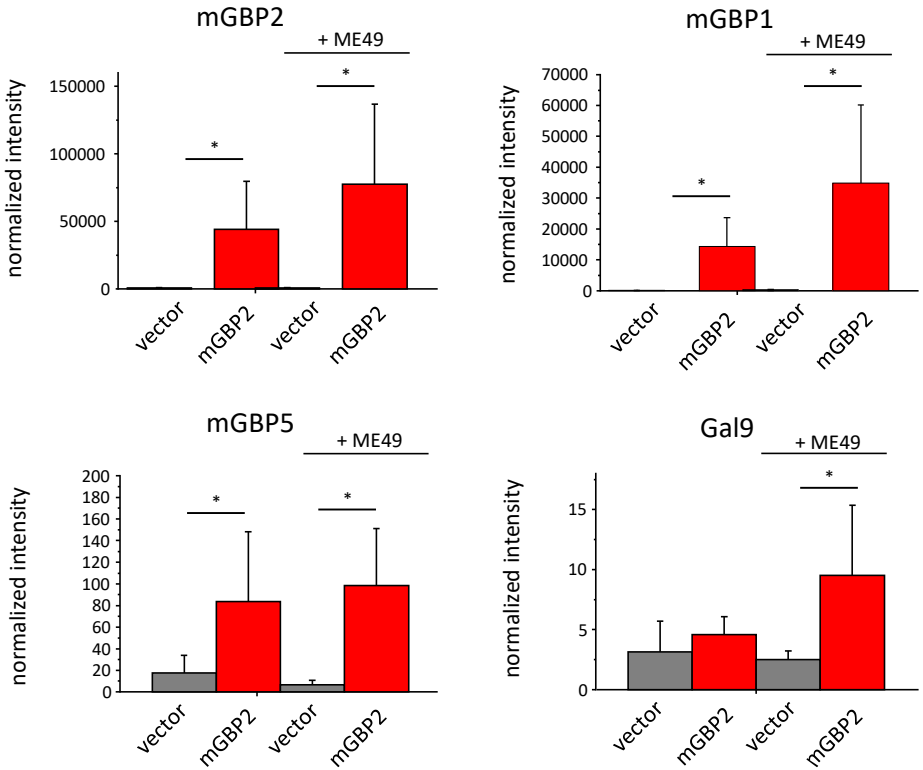

					-				ME49			
accession	gene names	score		count	p-value	q-value mGBP2/control	ratio	significance mGBP2/control	p-value	q-value mGBP2/control	ratio	significance mGBP2/control
Q01514	mGBP1	1702.6	19	19	3.3E-08	0	186	+	2.8E-06	0	199.7	+
Q9Z0E6	mGBP2	4193.6	55	55	1.3E-07	0	66.8	+	1.5E-06	0	125.4	+
Q8CFB4	mGBP5	199.1	6	6	9.1E-03	0.0105263	4.8	+	6.3E-05	0	15.1	+
O08573	Gal9	79.9	2	2	1.3E-01	0.251424	1.5		5.6E-03	0.00446061	3.8	+

mGBP2$^{-/-}$MEFs + *T. gondii* 4 h

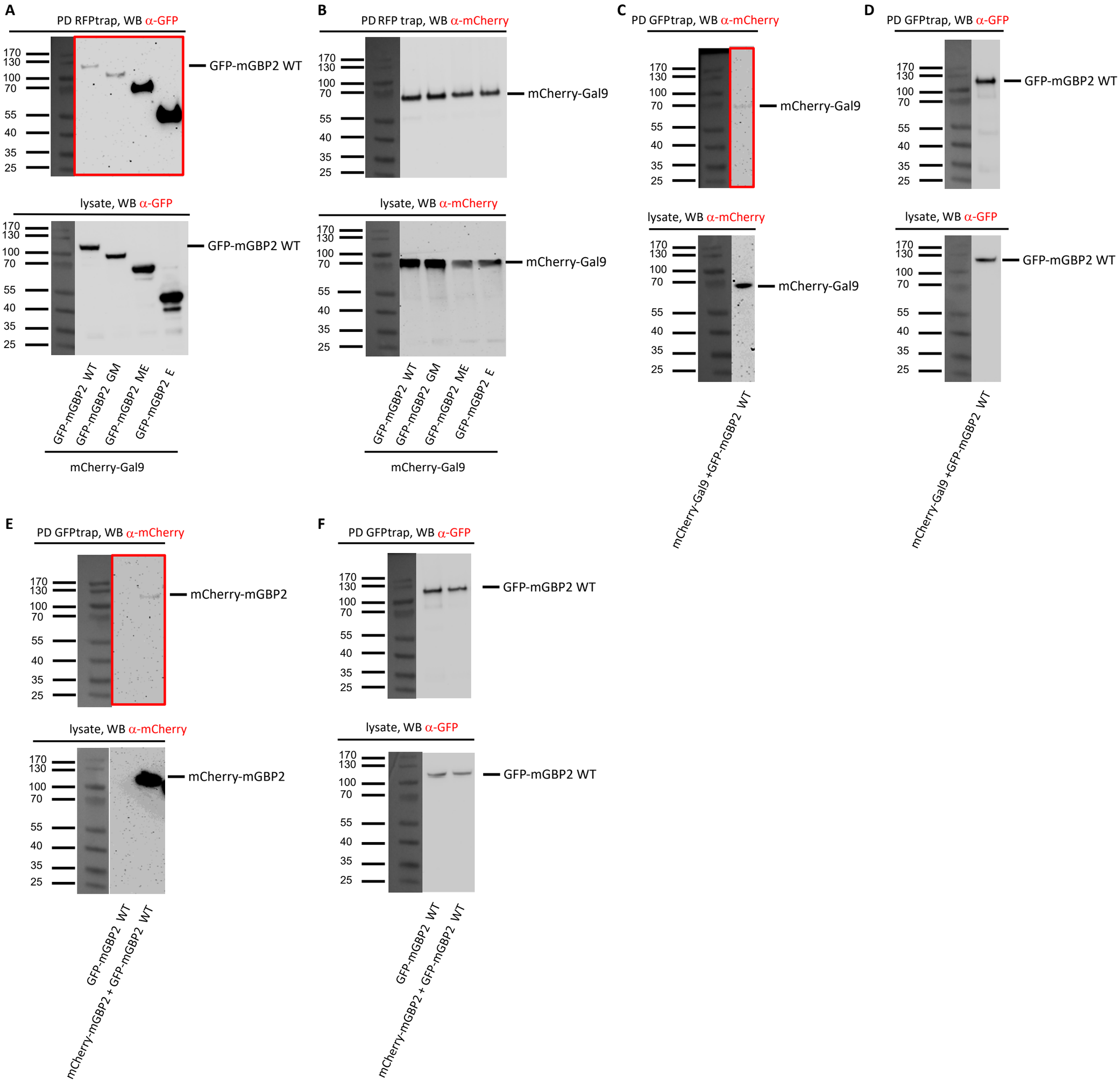

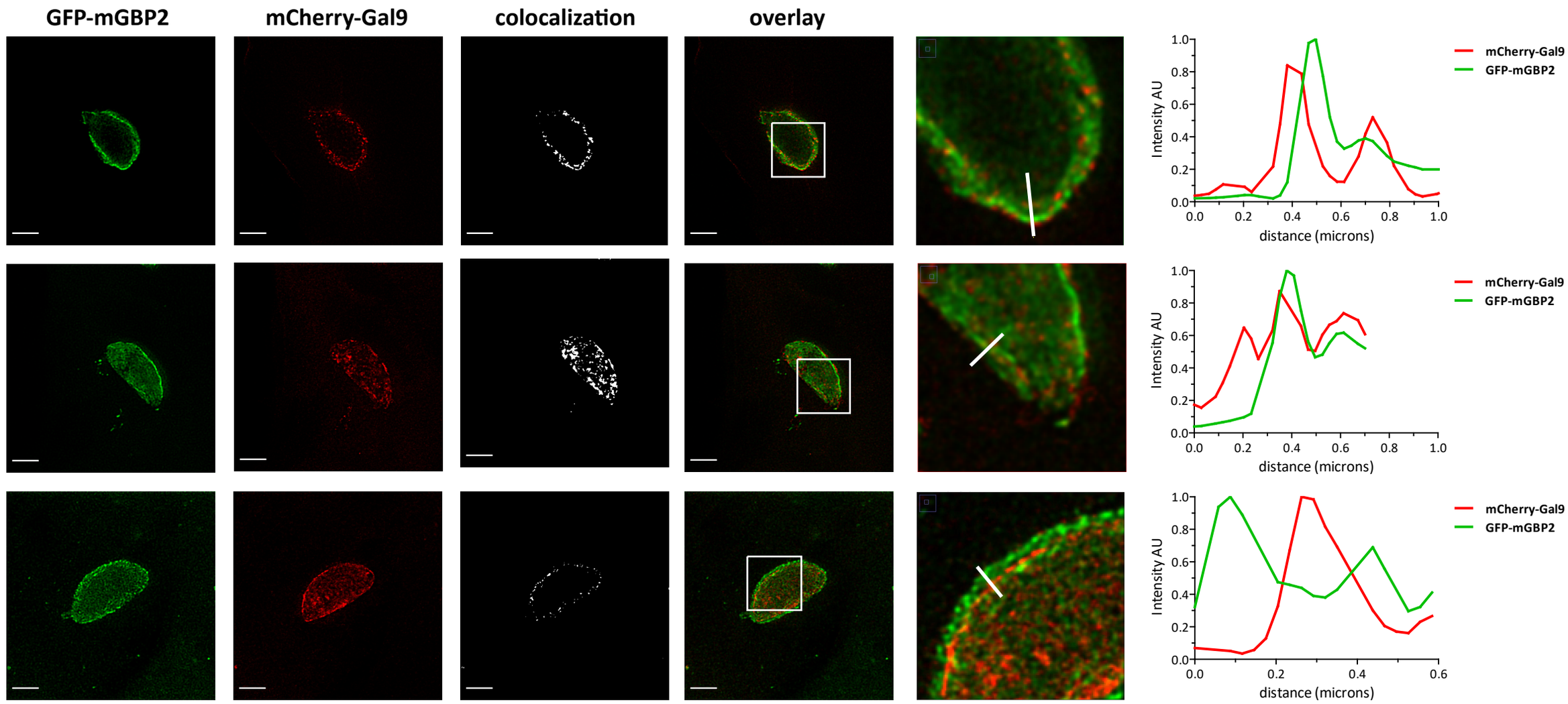
GFP-mGBP2
mCherry-Gal9
colocalization
overlay
Intensity AU
distance (microns)
mCherry-Gal9
GFP-mGBP2

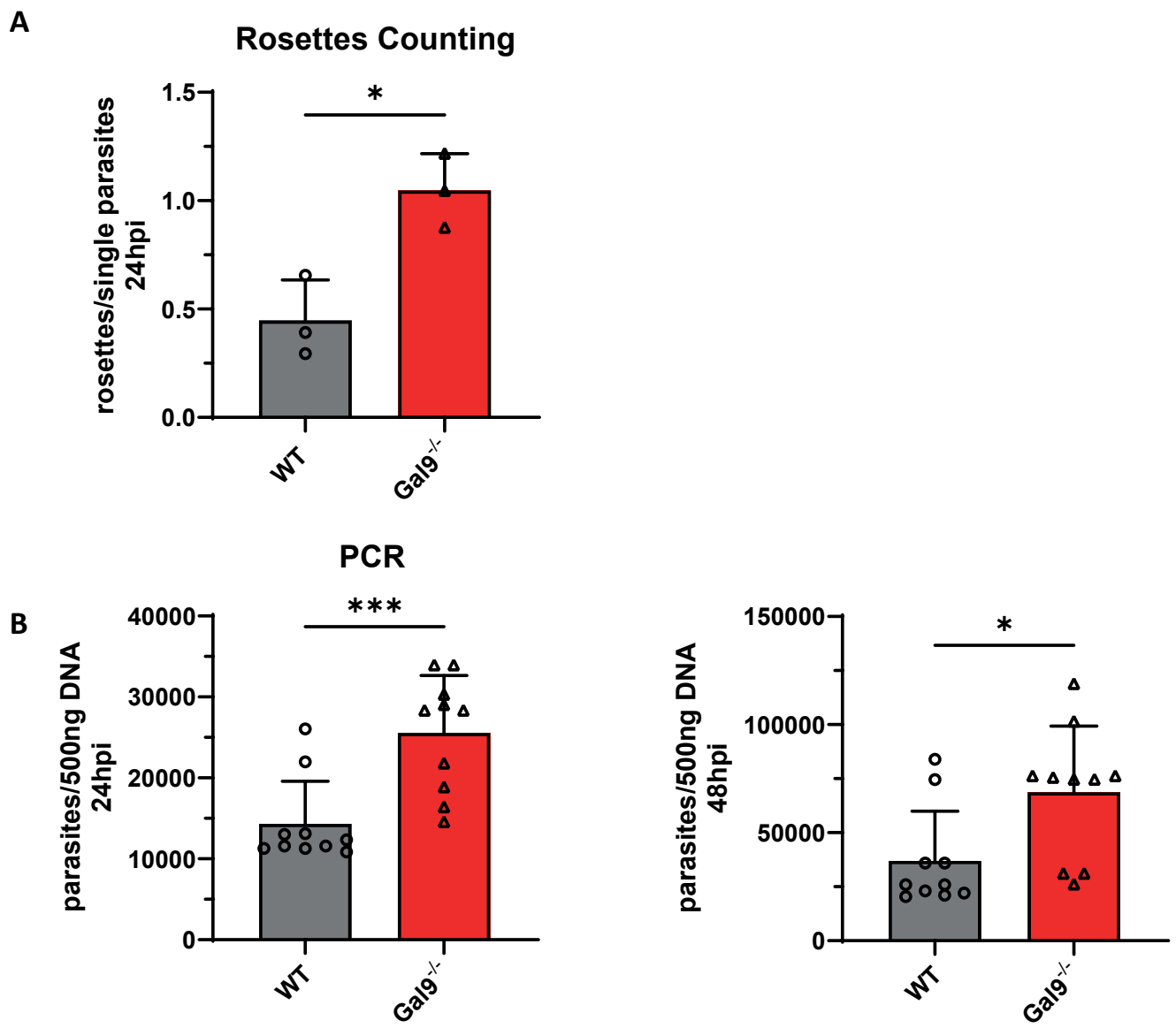
A
Rosettes Counting
rosettes/single parasites 24hpi
1.5
1.0
0.5
0.0
*
WT
Gal9-/-
PCR
B
parasites/500ng DNA 24hpi
40000
30000
20000
10000
0
***
WT
Gal9-/-
parasites/500ng DNA 48hpi
150000
100000
50000
0
*
WT
Gal9-/-